ACS NANO

ARTICLE

Lithographically Patterned Functional Polymer–Graphene Hybrids for Nanoscale Electronics

Hadas Alon,[†,‡,§] Chen Stern,[‡,§] Moshe Kirshner,[‡,§] Ofer Sinai,[‡,§] Michal Wasserman,[‡,§] Ryan Selhorst,[∥] Raymond Gasper,[⊥] Ashwin Ramasubramaniam,[#] Todd Emrick,[∥] and Doron Naveh*,[‡,§]

[†]Department of Chemistry and [‡]Faculty of Engineering, Bar-Ilan University, Ramat-Gan 52900, Israel
[§]Bar-Ilan Institute for Nanotechnology and Advanced Materials, Ramat-Gan 52900, Israel
[∥]Polymer Science and Engineering Department, [⊥]Department of Chemical Engineering, and [#]Department of Mechanical and Industrial Engineering, University of Massachusetts, Amherst, Massachusetts 01003, United States

S *Supporting Information*

ABSTRACT: Two-dimensional (2D) materials are believed to hold significant promise in nanoscale optoelectronics. While significant progress has been made in this field over the past decade, the ability to control charge carrier density with high spatial precision remains an outstanding challenge in 2D devices. We present an approach that simultaneously addresses the dual issues of charge-carrier doping and spatial precision based on a functional lithographic resist that employs methacrylate polymers containing zwitterionic sulfobetaine pendent groups for noncovalent surface doping of 2D materials. We demonstrate scalable approaches for patterning these polymer films *via* electron-beam lithography, achieving precise spatial control over carrier doping for fabrication of high-quality, all-2D, lateral p−n junctions in graphene. Our approach preserves all of the desirable structural and electronic properties of graphene while exclusively modifying its surface potential. The functional polymer resist platform and concept offers a facile route toward lithographic doping of graphene- and other 2D material-based optoelectronic devices.

KEYWORDS: *graphene, doping, p−n junction, psbma, interface, zwitterion*
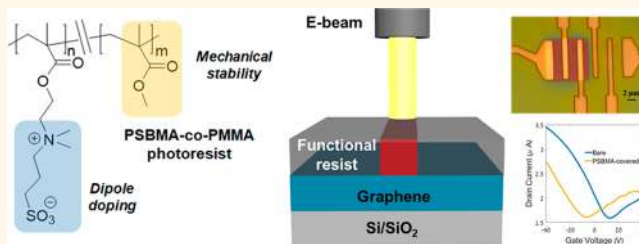
Two-dimensional (2D) materials exhibit important physical and electronic properties and are poised to benefit optoelectronic technologies and emerging electronic device paradigms. Due to their relatively high carrier mobilities and long-term environmental stability, 2D electronic materials are promising alternatives to organic semiconductors in the fields of printable and flexible electronics.[1] While much progress has been made in the fabrication of 2D-materials based devices, the ability to exercise precise spatial control over majority carrier type and concentration remains an outstanding challenge that must be overcome for engineering integrated circuits and systems. In this work, we design a hybrid polymer–graphene platform for carrier doping of graphene *via* noncovalent adsorption of functional polymer thin films. We demonstrate scalable approaches for patterning these polymer films *via* electron-beam lithography, achieving precise spatial control over carrier doping for fabrication of lateral homojunctions. Our approach preserves all of the desirable structural and electronic properties of graphene, while exclusively modifying its surface potential, and offers a facile route toward lithographic doping of graphene-based devices.

Graphene is a special case of a zero-bandgap 2D semiconductor that poses challenges for nanoscale electronics while simultaneously affording scientific and technological opportunities. Numerous modern electronic devices utilize semiconductors as their basic building blocks and cannot be fabricated with gapless graphene. Nonetheless, the unique electronic properties of graphene allow for emerging device architectures beyond traditional semiconductor electronics.[2] For example, analogous to wave-guiding in ray optics, p−n junctions in graphene can guide ballistic carrier currents;[3] this functionality exploits the unusual angle-dependent conductance of graphene junctions to achieve phenomena such as electron focusing and collimation.[4,5] In some cases, ballistic graphene devices operate in a manner similar to analog electronic multiplexers.[2,6,7] Graphene p−n junctions also display unusual light-matter interactions including the photo-thermoelectric
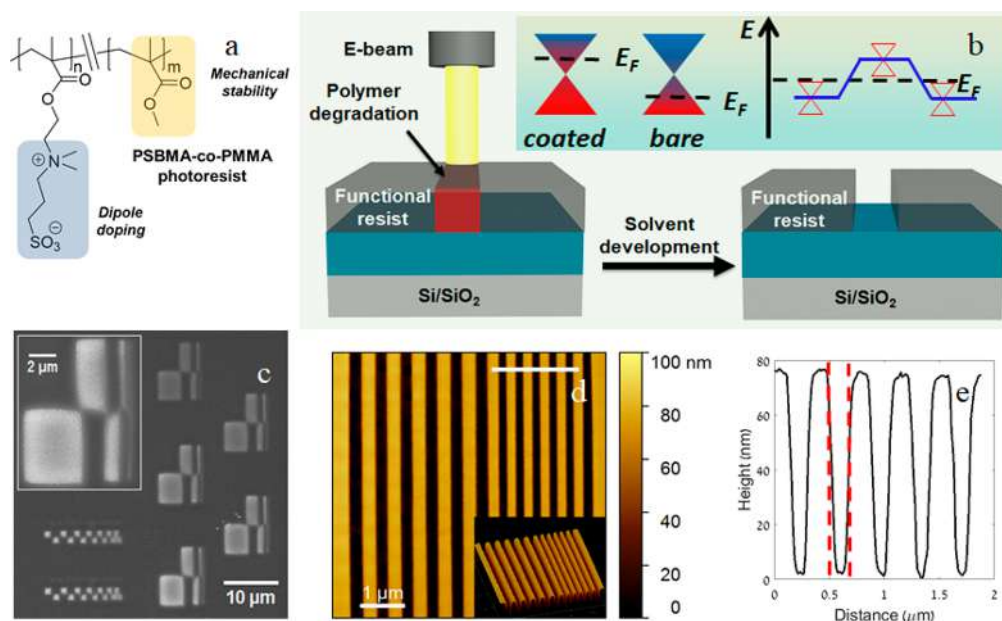
Figure 1. Chemical structure of poly(sulfobetaine-co-methyl)methacrylate used in this work (i.e., P(SBMA-co-MMA) (a), and its patterning process with electron beam and the resulting shift in chemical potential (b). Dose and resolution calibration charts optimized to 100 nm features (c) and atomic force micrograph of lines defined on PSBMA-co-PMMA resist with 30 keV electron beam (d) with its cross-section along the white line shown in topographic map (e).

effect[8] and self-driven, bias-free photocurrents.[9] Thus, there is significant interest in developing precise and scalable methods for area-selective carrier doping of graphene for realizing novel 2D optoelectronic devices.

In this work, we present a hybrid graphene−functional polymer (hard−soft materials) platform that simultaneously addresses the dual issues of carrier doping and scalable device processing. Specifically, we exploit the extreme sensitivity of graphene to its immediate environment and engineer suitable zwitterionic polymers that induce appreciable surface potential shifts in graphene via adsorbed interfacial dipoles. A key feature of these polymers is that the zwitterionic moieties are incorporated as pendent groups attached to poly(methyl methacrylate) (PMMA) backbones, rendering them amenable to patterning via electron-beam lithography. We note that other molecules[10] and polymers (e.g., poly(4-vinylpyridine) and poly(vinyl chloride)[11]) have been utilized in the past for doping graphene, with complementary doping achieved via rubber-stamping of bis(trifluoromethanesulfonyl) and poly-(ethylene imine).[12] The key innovation in our work is the development of lithographically processed polymer dopant that can be directly patterned on the target undoped material for achieving carrier density control at high spatial resolution.

RESULTS AND DISCUSSION

Noncovalent adsorption of dopant moieties is an attractive approach for modulating the electronic properties of 2D materials while preserving their overall structural integrity and purity and therefore provide significant advantages over ion implantation methods.[13] Here, we employ methacrylate polymers containing zwitterionic sulfobetaine (SB) pendent groups for contact with graphene. The SB moiety incorporates a sulfonate anion and ammonium cation with a net dipole moment of 15.2 D, as estimated from density functional theory (DFT) calculations. Prior studies by Emrick and co-workers showed that PSBMA thin films significantly reduced the work

function of ITO, Au, Al and graphene (by 1.09, 1.52, 0.36, and 1.64 eV, respectively),[14] which motivates the use of these polymers to design functional lithographic resists. Moreover, the zwitterion concentration is an important knob for adjusting the PSBMA-induced work-function shift and therefore is a strong motivator for applying our copolymer method of doping.[14] Briefly, the zwitterionic P(SBMA-co-MMA) was synthesized by conventional (azo-alkane initiated) free radical polymerization in trifluoroethanol (TFE), as shown in Figure 1. Monomer conversion, monitored by ^{1}H NMR spectroscopy, after 6 h at 70 °C approached 60−70% matched the targeted feed ratio. The molecular weight of the polymer was 54 kDa, as estimated by gel permeation chromatography (GPC) in TFE, and the polydispersity value was ∼1.4. The solution processability of the polymer is pertinent to the design and implementation of resists for lithographic patterning. Sulfobe-taine imparts solubility to the PMMA copolymer in salt water, TFE, and polar aprotic solvents such as N-methyl pyrollidone (NMP). This advantageous solubility, coupled with high molecular weight, makes this polymer an excellent candidate for lithographic processing on substrates.

The synthesized copolymer with a 1:1 ratio of SBMA/MMA ratio was optimized as a solution-processable positive tone resist with respect to exposure dosage (30 keV e-beam) and development conditions to achieve patterned functional films of 80 nm thickness and 200 nm line width and pitch (Figure 1b). Figure 1c displays an atomic force micrograph of a patterned resist showing sharp topography maps of 10 μm long lines of 200−300 nm width and pitch. The level of spatial resolution achieved with our resist is comparable to that of commercial PMMA resists when processed with the same beam energy and resist thickness; the key difference is that our P(SBMA-co-MMA) photoresist is a functional resist that can n-dope graphene.

The doping effect of the PSBMA-co-PMMA photoresist on graphene was studied by Raman spectroscopy. Figure 2a
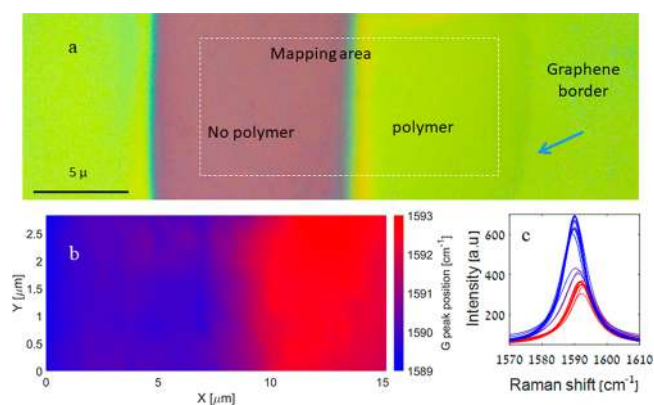
Figure 2. Optical micrograph of a graphene−PSBMA hybrid (a); Raman mapping of the G-peak (b) scanned over marked area in (a) and representative spectra from the bare (blue) and PSBMA-covered areas (red).

displays an example of the polymer photoresist applied by spin coating to a 40 μm × 10 μm monolayer of CVD-grown graphene (on Si/SiO$_2$), patterned by e-beam writing, then developed with solvent to coat only the right half of the flake. Thereafter, local chemical potential shifts of graphene in the polymer-coated and bare regions were inferred by mapping the optical phonon (G-mode) energy *via* Raman spectroscopy. The Raman G peak of graphene arises from bond stretching of all pairs of sp^2 atoms and is a signature of the number and quality of layers, doping level, and confinement.[15,16] Parts b and c of Figure 2 display a Raman map of the entire graphene monolayer as well as individual line scans taken along the length of the monolayer from which we observe a clear shift in the G-peak frequency from 1589 cm^{-1} in the uncoated region to 1593 cm^{-1} in the polymer-coated part; the frequency shift clearly results from the resist pattern. This shift in the optical phonon energy indicates a change in carrier concentration with respect to the neutrality point.[17] However, these doping-induced shifts do not shed light on the carrier type; to glean this information, we turn to transport measurements.

Measurements of gate-resolved conductivity of graphene field-effect transistors (FETs) provide precise values of the average carrier density induced by the functional polymer in the graphene monolayer. Specifically, the average carrier density, $\bar{n}$, is given by $\bar{n} = C_g[V_g − V_{CNP}]/e$, where C_g is the gate capacitance and V_g and V_{CNP} are the gate and neutrality point voltages, respectively. We prepared a series of five FETs on a single-monolayer of CVD graphene (Figure 3a): two devices were unexposed by lithography and therefore remained coated with the functional polymer dopant, two devices were exposed and developed to measure transport in the bare graphene region, and one device spanned the functionalized and bare graphene regions effectively measuring transport across a homojunction. Control experiments were also performed on bare- and PMMA-coated graphene devices to confirm the absence of unintentional, process-related doping effects from PMMA (see the SI for details). In comparing the charge-neutrality voltage (Figure 3), we observe a shift of ∼20 V (over 285 nm of Si/SiO$_2$) between the coated and uncoated devices. This shift in the charge neutrality point of graphene induced by the P(SBMA-*co*-MMA) resist corresponds to a doping level of 1.35 × 10^{12} cm^{-2} and a Fermi-level shift determined by $\phi = \sin(V_g − V_{CNP})\hbar v_F\sqrt{\pi|\bar{n}|}$ where $\nu_F = 10^6$ m/s is the Fermi velocity of carriers in graphene and $\bar{n}$ is the effective doping level.[18] Furthermore, comparing the device characteristics of the bare FETs *versus* the polymer-coated ones (see Figures S2 and S3) reveals two important conclusions: (i) our surface functionalization method produces uniform carrier doping over the polymer-coated regions and (ii) the field-effect mobility of charge carriers is barely affected upon surface functionalization, which indicates negligible introduction of charged impurities from the polymer film.

The ability of P(SBMA-*co*-MMA) to produce lateral graphene homojunctions is seen in the device characteristics in Figure 3d that show the distinct I−V signature of a p−n junction. We attribute the formation of this p-n homojunction to the potential shift induced within the polymer-coated graphene region by the SB molecular dipole moment. From
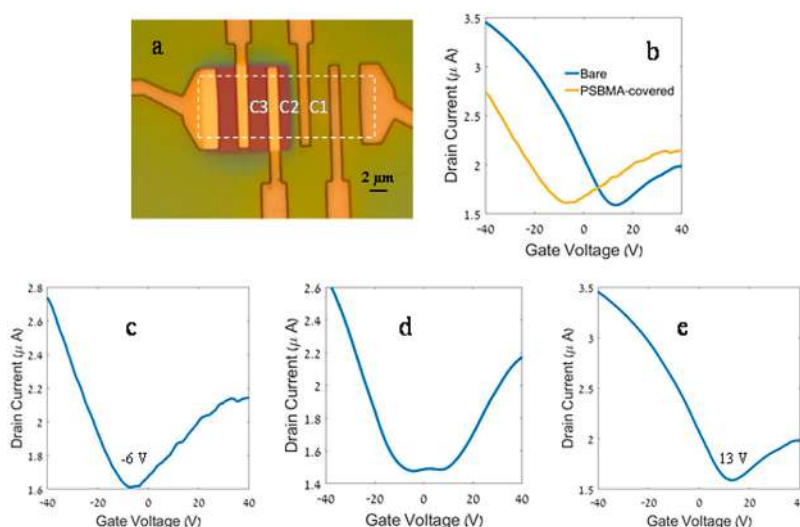
Figure 3. (a) Optical micrograph of hybrid graphene−PSBMA device consisting of monolayer graphene partially covered with PSBMA (green region). (b) Gate-resolved I−V curves taken from the PSBMA-covered and bare regions of the device (yellow and blue lines, respectively). (c−e) I−V curves of the three central devices shown in the optical micrograph namely, the PSBMA-covered device (C1), the p−n junction (C2), and the bare device (C3).
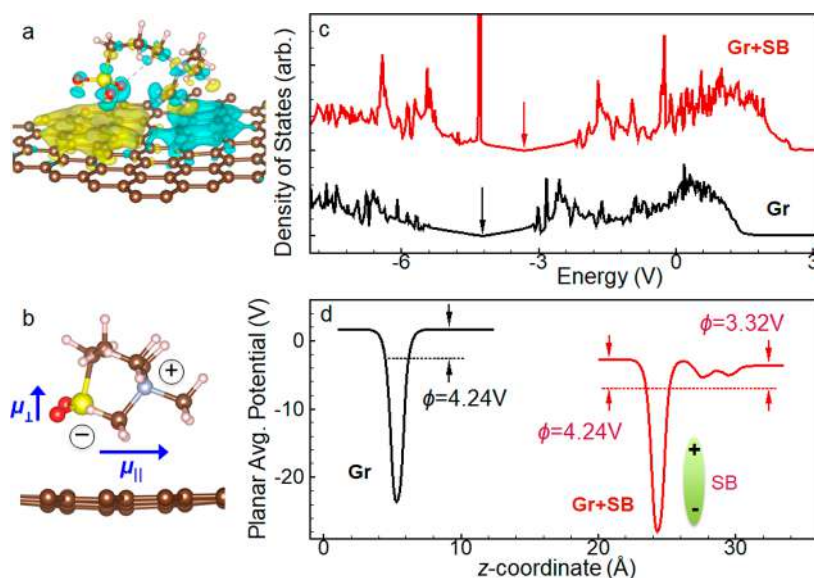
Figure 4. (a) Charge-transfer plot for a sulfobetaine (SB) pendent group on a graphene sheet; yellow/cyan isosurfaces ($\pm 3 \times 10^{-3}$ e/Å^3) indicate charge accumulation/depletion. (b) Side view of SB group on graphene sheet: the tilted adsorption configuration of the pendent group leads to both transverse ($\mu_{\parallel}$) and normal ($\mu_{\perp}$) components of the surface dipole. (c) Total density of states of a bare graphene sheet (Gr) and of a graphene sheet with an adsorbed SB pendent group (Gr + SB). All energies are reported relative to the vacuum level (0 V); arrows indicate the location of the charge-neutrality point of graphene that is seen to shift toward higher energies upon adsorption of the SB group. (d) Planar averaged Hartree potential along z-direction (normal to graphene sheet) for bare graphene (Gr) and a graphene sheet with adsorbed SB (Gr + SB); the oscillations in the potential for the latter case are due to the adsorbed SB group, which is indicated schematically. Dotted lines indicate the position of the Fermi level from which we infer the indicated work functions (φ) with respect to the vacuum potential. The plots in (c) and (d) are shifted arbitrarily relative to each other for clarity. (Atom colors: C, brown; S, yellow; N, blue; O, red; H, white).

basic electrostatics,[19] the shift in surface potential of polymer-coated graphene is $\Delta\phi = -\frac{qD}{\varepsilon_0 \varepsilon_{eff}}$, where $D = \rho\mu_{\perp}$ is the dipole moment per unit area of polymer−graphene interface, ρ is the area density of dipoles at the polymer−graphene interface, $\mu_{\perp}$ is the component of the zwitterion molecular dipole moment normal to the graphene sheet, and ε_{eff} is the effective dielectric constant of the embedding medium (SiO$_2$ and polymer) defined by $\varepsilon_{eff} = [\varepsilon_{SiO2} + \varepsilon_{polymer}]/2$. Specific to our case, the functional resist contains 0.16 M units of zwitterions corresponding to an area density of $\rho \approx 2.1 \times 10^{13}$ cm^{-2} at the polymer−graphene interface. With the measured Fermi level shift of $\Delta\phi \approx 0.2$ eV and an effective dielectric constant of $\varepsilon_{eff} \approx 4$, we arrive at an estimate of $\mu_{\perp} \approx 10D$ for the molecular dipole moment of adsorbed SB moieties.

To further understand the physical and electronic interactions between the polymer thin film and graphene, we performed first-principles density functional theory (DFT) calculations using the Vienna Ab Initio Simulation Package (VASP).[20,21] While it is impractical to model the adsorbed polymer chains in their entirely, important insights can be gained by considering the key components of the system, namely, the SB pendent group and the graphene sheet. Our computational model thus consists of a 6 × 6 graphene supercell on which we adsorb the SB pendent groups. As seen from Figure 4a,b, the SB moiety adsorbs in a flat configuration—interacting with the graphene sheet via the terminal sulfate and methyl groups—with a calculated binding energy of 0.92 eV, indicative of a stable polymer−graphene interface. Figure 4a displays the transfer of charge between the SB pendent group and the graphene sheet; as expected, the oppositely charged ends of the zwitterionic moiety induce corresponding regions of electron accumulation and depletion

within the graphene monolayer. The charge redistribution within the graphene monolayer is fairly localized, extending but a few unit cells beyond the adsorbed SB group, and is clearly not long-ranged. On average though, the induced positive and negative charges within the graphene sheet cancel each other, and unlike our previous work on TTF pendent groups adsorbed on MoS$_2$,[22] there is no net charge transfer between graphene and SB. The bonding mechanism between the SB pendent group and the graphene sheet is thus primarily via noncovalent and localized charge-transfer interactions.

We further observe from Figure 4b that the S and N atoms are at slightly different heights from the graphene sheet in the adsorbed configuration. This surface dipole may be further decomposed into components transverse and normal to the graphene sheet. The transverse components of the dipoles of randomly adsorbed SB pendent groups will, on average, cancel out and contribute only to short-range scattering mechanisms; the normal components are, however, additive leading to a net dipole moment normal to the graphene sheet ($\mu_{\perp} = 4.7D$). This surface dipole induces a shift in the charge-neutrality point of the graphene sheet toward the vacuum level as seen from the density of states plot in Figure 4c. Correspondingly, the planar-averaged DFT local potential in Figure 4d shows a reduced work function of the graphene sheet on the side with the adsorbed SB moiety ($\phi = 3.32$ eV) relative to the side without the surface dipole (equivalently, the bare graphene sheet; $\phi = 4.24$ eV). While the DFT calculation does not take into account dielectric screening from the substrate and polymer film, as a first approximation the work function shift, $\Delta\phi_{DFT} = 0.92$ eV, may be renormalized simply by the effective dielectric constant of the embedding medium, $\varepsilon_{eff} \approx 4$, which leads to a predicted work function shift of $\Delta\phi_{predicted} = 0.23$ eV. This excellent

quantitative agreement between theory and experiment bolsters the view of purely noncovalent electrostatic interactions between the functional polymer and graphene. An immediate consequence of this electrostatic picture of polymer−graphene interactions is that the zwitterion concentration can be tuned *a priori* to induce desired Fermi level shifts in graphene, which will be studied elsewhere.

CONCLUSIONS

In conclusion, we have demonstrated a scalable and precise approach for fabricating hybrid polymer−graphene nanoscale devices. Beyond graphene, the ability to dope other 2D materials—including semiconductors such as transition-metal dichalcogenides and phosphorene, among others—in a controlled manner can be pivotal for the development of nanoscale optoelectronic devices. The patterning and synthetic methods developed in this work can be extended more generally to other 2D materials and, in conjunction with polymer dielectric substrates, could offer a path towards low-power, flexible 2D-materials-based electronics.

METHODS

Graphene Synthesis and Device Fabrication. Graphene was transferred to p-type silicon wafer with 285 nm oxide layer. The graphene was synthesized by CVD as described by others with some adaptations (ref 23). For graphene transfer, the copper was etched by ammonium persulfate (Merck, >98%). The graphene layer was formed into the desired shapes using AZ nLOF 2020 negative tone resist followed by oxygen plasma etch. On the top of the graphene bar, six electrodes (Ti/Pd 5/55 nm) were patterned by electron-beam lithography using PMMA and metallized by electron-beam evaporation followed by lift off.

PSBMA−PMMA Copolymer Synthesis and Characterization. Sulfobetaine methacrylate, methyl methacrylate, 2,2-azobisisobutyrylnitrile, and methanol were purchased from Aldrich. 2,2,2-Trifluoroethanol was purchased from TCI chemicals. AIBN was recrystallized from toluene and MMA was run through a plug of basic alumina to remove the inhibitor before use. All other reagents were used as received.

Polymer Synthesis. Into a 25 mL round-bottom flask were added SBMA (1.0 g, 3.6 mmol), MMA (0.36 g, 3.6 mmol), and AIBN (7.0 mg, 0.045 mmol) in TFE (14 mL). The solution was degassed under nitrogen atmosphere for 30 min and then heated to 70 °C in an oil bath. The mixture stirred at 70 °C for 6 h and then was quenched by exposure to ambient atmosphere. The resulting solution was precipitated into methanol, and the solid was collected by centrifugation and then was washed several times with methanol. The solid was then dried under vacuum and lyophilized to remove excess water. Yield: 0.75 g, 55%. The molecular weight of the polymer was 54 kDa, measured by gel permeation chromatography (GPC) in TFE, with polymer dispersity of 1.4. Spectroscopic data are given in the SI.

Patterning of PSBMA−PMMA copolymer. A solution of 10 mg PSBMA−PMMA copolymer was dissolved in 1 mL of TFE. The solution was stirred for 72 h at room temperature before use. The sample was spin-coated with the solution (500 rpm/5 s, 3000 rpm/45 s) and baked for 2 min at 120 °C on a hot plate. The polymer was exposed to a 30 kV e-beam (VEGA3, Tescan) with a dosage of 1200 μC/cm^2 and developed in preheated NMP (100 °C) for 3 min (for a clean silicon substrate) or 1 min (for a silicon/graphene substrate) followed by 30 s in air (allowing the sample to cool down gradually), soaked for 30 s in IPA, and blow-dried by nitrogen flow.

AFM Measurement. Data were collected using a Bio FastScan AFM (Bruker, AXS, Santa Barbara, CA).

Raman Characterization. Silicon wafers containing graphene or patterned graphene (10 μm windows of the PSBMA−PMMA copolymer) were placed in a vacuum chamber (HFS600E-PB4,

Linkam Scientific Instruments). Raman spectra were measured using a Raman microscope (LabRAM HR Evolution, HORIBA Scientific) with a 532 nm laser. Mapping data were fit to Lorentzian functions using a custom Matlab script.

Electrical Measurement. Samples were wire bonded to a ceramic leadless chip carrier and then placed and measured in a vacuum chamber (Montana Instruments) for measurements using a Keithley 2540 or Keysight B1500A. All presented data were collected at room temperature.

Computational Data. Non-spin-polarized, planewave DFT calculations were performed using the Vienna *Ab Initio* Simulation Package (VASP).[20,21] The core and valence electrons were treated using the projector-augmented wave method.[21,24] The Perdew−Burke−Ernzerhof (PBE) generalized-gradient approximation was used to describe electron exchange and correlation.[25] van der Waals interactions were approximated *via* the zero-damping DFT D3 method of Grimme *et al.*[26] From convergence studies, a kinetic energy cutoff of 400 eV was chosen. Electronic convergence was accelerated with a Gaussian smearing of 0.01 eV for relaxation calculations; the Blöchl tetrahedron method[27] was used thereafter for calculating density of states and the local potential. All systems had between 12 and 15 Å of vacuum normal to the graphene layer to prevent spurious interaction between images. Dipole corrections were applied normal to the graphene monolayer along the vacuum direction. Atomic positions and in-plane cell dimensions were relaxed with a force tolerance of 0.02 eV/ Å. For relaxation calculations, the Brillouin zone was sampled with a 3 × 3 × 1 Γ-centered k-point mesh, determined to be sufficient from convergence studies. For single-point electronic structure calculations, after relaxation, the Brillouin zone was sampled with a 13 × 13 × 1 Γ-centered k-point mesh.

ASSOCIATED CONTENT

Ⓢ Supporting Information

The Supporting Information is available free of charge on the ACS Publications website at DOI: 10.1021/acsnano.7b08844.

> Synthetic methods and characterization of the polymer; electrical measurements and control experiments of devices covered with pure PMMA; odd resistance and conductivity of p−n junction (PDF)

AUTHOR INFORMATION

Corresponding Author

*E-mail: doron.naveh@biu.ac.il.

ORCID Ⓞ

Ashwin Ramasubramaniam: 0000-0001-6595-7442

Todd Emrick: 0000-0003-0460-1797

Doron Naveh: 0000-0003-1091-5661

Author Contributions

The manuscript was written through contributions of all authors. H.A., O.S., and M.W. developed the protocol for the resist processing with electron-beam lithography, H.A. fabricated and characterized devices, M.K. and O.S. assisted in electrical measurements and Raman data processing, C.S. synthesized graphene and prepared samples, R.S. and T.E. synthesized and characterized PSBMA copolymer, R.G. and A.R. conducted the computational analysis, and D.N. conceived and supervised the study.

Notes

The authors declare no competing financial interest.

ACKNOWLEDGMENTS

REFERENCES

(1) Nathan, A.; Ahnood, A.; Cole, M. T.; Lee, S.; Suzuki, Y.; Hiralal, P.; Bonaccorso, F.; Hasan, T.; Garcia-Gancedo, L.; Dyadyusha, A. Flexible Electronics: The Next Ubiquitous Platform. *Proc. IEEE* **2012**, *100* (Special Centennial Issue), 1486−1517.

(2) Tanachutiwat, S.; Lee, J. U.; Wang, W.; Sung, C. Y. Reconfigurable Multi-Function Logic Based on Graphene pn Junctions. *Proc. 47th Design Automation Conf., ACM* **2010**, 883−888.

(3) Williams, J. R.; Low, T.; Lundstrom, M. S.; Marcus, C. M. Gate-Controlled Guiding of Electrons in Graphene. *Nat. Nanotechnol.* **2011**, *6*, 222−225.

(4) Cheianov, V. V.; Fal'ko, V.; Altshuler, B. The Focusing of Electron Flow and a Veselago Lens in Graphene pn Junctions. *Science* **2007**, *315*, 1252−1255.

(5) Park, C.-H.; Son, Y.-W.; Yang, L.; Cohen, M. L.; Louie, S. G. Electron Beam Supercollimation in Graphene Superlattices. *Nano Lett.* **2008**, *8*, 2920−2924.

(6) Barnard, A. W.; Hughes, A.; Sharpe, A. L.; Watanabe, K.; Taniguchi, T.; Goldhaber-Gordon, D. Absorptive Pinhole Collimators for Ballistic Dirac Fermions in Graphene. *Nat. Commun.* **2017**, *8*, 15418.

(7) Chen, S.; Han, Z.; Elahi, M. M.; Habib, K. M. M.; Wang, L.; Wen, B.; Gao, Y.; Taniguchi, T.; Watanabe, K.; Hone, J.; Ghosh, A. W.; Dean, C. R. Electron Optics with p-n Junctions in Ballistic Graphene. *Science* **2016**, *353*, 1522−1525.

(8) Gabor, N. M.; Song, J. C.; Ma, Q.; Nair, N. L.; Taychatanapat, T.; Watanabe, K.; Taniguchi, T.; Levitov, L. S.; Jarillo-Herrero, P. Hot Carrier−Assisted Intrinsic Photoresponse in Graphene. *Science* **2011**, *334*, 648−652.

(9) Lemme, M. C.; Koppens, F. H.; Falk, A. L.; Rudner, M. S.; Park, H.; Levitov, L. S.; Marcus, C. M. Gate-Activated Photoresponse in a Graphene p−n Junction. *Nano Lett.* **2011**, *11*, 4134−4137.

(10) Georgakilas, V.; Otyepka, M.; Bourlinos, A. B.; Chandra, V.; Kim, N.; Kemp, K. C.; Hobza, P.; Zboril, R.; Kim, K. S. Functionalization of Graphene: Covalent and Non-Covalent Approaches, Derivatives and Applications. *Chem. Rev.* **2012**, *112*, 6156−6214.

(11) Lee, S. K.; Yang, J. W.; Kim, H. H.; Jo, S. B.; Kang, B.; Bong, H.; Lee, H. C.; Lee, G.; Kim, K. S.; Cho, K. Inverse Transfer Method Using Polymers with Various Functional Groups for Controllable Graphene Doping. *ACS Nano* **2014**, *8*, 7968−7975.

(12) Choi, Y.; Sun, Q.; Hwang, E.; Lee, Y.; Lee, S.; Cho, J. H. On-Demand Doping of Graphene by Stamping with a Chemically Functionalized Rubber Lens. *ACS Nano* **2015**, *9*, 4354−4361.

(13) Shlimak, I.; Haran, A.; Zion, E.; Havdala, T.; Kaganovskii, Y.; Butenko, A. V.; Wolfson, L.; Richter, V.; Naveh, D.; Sharoni, A.; Kogan, E.; Kaveh, M. Raman Scattering and Electrical Resistance of Highly Disordered Graphene. *Phys. Rev. B: Condens. Matter Mater. Phys.* **2015**, *91*, 045414.

(14) Lee, H.; Puodziukynaite, E.; Zhang, Y.; Stephenson, J. C.; Richter, L. J.; Fischer, D. A.; DeLongchamp, D. M.; Emrick, T.; Briseno, A. L. Poly(Sulfobetaine Methacrylate)S as Electrode Modifiers for Inverted Organic Electronics. *J. Am. Chem. Soc.* **2015**, *137*, 540−549.

(15) Ferrari, A. C. Raman Spectroscopy of Graphene and Graphite: Disorder, Electron−Phonon Coupling, Doping and Nonadiabatic Effects. *Solid State Commun.* **2007**, *143*, 47−57.

(16) Das, A.; Pisana, S.; Chakraborty, B.; Piscanec, S.; Saha, S.; Waghmare, U.; Novoselov, K.; Krishnamurthy, H.; Geim, A.; Ferrari, A. Monitoring Dopants by Raman Scattering in an Electrochemically Top-Gated Graphene Transistor. *Nat. Nanotechnol.* **2008**, *3*, 210−215.

(17) Yan, J.; Zhang, Y.; Kim, P.; Pinczuk, A. Electric Field Effect Tuning of Electron-Phonon Coupling in Graphene. *Phys. Rev. Lett.* **2007**, *98*, 166802.

(18) Yu, Y.-J.; Zhao, Y.; Ryu, S.; Brus, L. E.; Kim, K. S.; Kim, P. Tuning the Graphene Work Function by Electric Field Effect. *Nano Lett.* **2009**, *9*, 3430−3434.

(19) Cahen, D.; Naaman, R.; Vager, Z. The Cooperative Molecular Field Effect. *Adv. Funct. Mater.* **2005**, *15*, 1571−1578.

(20) Kresse, G.; Furthmüller, J. Efficient Iterative Schemes for *Ab Initio* Total-Energy Calculations Using a Plane-Wave Basis Set. *Phys. Rev. B: Condens. Matter Mater. Phys.* **1996**, *54*, 11169−11186.

(21) Kresse, G.; Joubert, D. From Ultrasoft Pseudopotentials to the Projector Augmented-Wave Method. *Phys. Rev. B: Condens. Matter Mater. Phys.* **1999**, *59*, 1758−1775.

(22) Selhorst, R. C.; Puodziukynaite, E.; Dewey, J. A.; Wang, P.; Barnes, M. D.; Ramasubramaniam, A.; Emrick, T. Tetrathiafulvalene-Containing Polymers for Simultaneous Non-Covalent Modification and Electronic Modulation of Mos 2 Nanomaterials. *Chem. Sci.* **2016**, *7*, 4698−4705.

(23) Yu, Q.; Jauregui, L. A.; Wu, W.; Colby, R.; Tian, J.; Su, Z.; Cao, H.; Liu, Z.; Pandey, D.; Wei, D.; Chung, T. F.; Peng, P.; Guisinger, N. P.; Stach, E. A.; Bao, J.; Pei, S.-S.; Chen, Y. P. Control and Characterization of Individual Grains and Grain Boundaries in Graphene Grown by Chemical Vapour Deposition. *Nat. Mater.* **2011**, *10*, 443−449.

(24) Blöchl, P. E. Projector Augmented-Wave Method. *Phys. Rev. B: Condens. Matter Mater. Phys.* **1994**, *50*, 17953−17979.

(25) Perdew, J. P.; Burke, K.; Ernzerhof, M. Generalized Gradient Approximation Made Simple. *Phys. Rev. Lett.* **1996**, *77*, 3865−3868.

(26) Grimme, S.; Antony, J.; Ehrlich, S.; Krieg, H. A Consistent and Accurate *Ab Initio* Parametrization of Density Functional Dispersion Correction (Dft-D) for the 94 Elements H-Pu. *J. Chem. Phys.* **2010**, *132*, 154104.

(27) Blöchl, P. E.; Jepsen, O.; Andersen, O. K. Improved Tetrahedron Method for Brillouin-Zone Integrations. *Phys. Rev. B: Condens. Matter Mater. Phys.* **1994**, *49*, 16223−16233.